Molecular Theory of Detonation Initiation: Insight from First Principles Modeling of the Decomposition Mechanisms of Organic Nitro Energetic Materials

Roman V. Tsyshevsky, Onise Sharia and Maija M. Kuklja *

MSE Department, University of Maryland, College Park, MD 20742, USA; rtsyshev@umd.edu (R.V.T.);
osharia@gmail.com (O.S.)

* Correspondence: mkukla@nsf.gov or mkukla@umd.edu; Tel.: +1-703-292-4940

Abstract: This review presents a concept, which assumes that thermal decomposition processes play a major role in defining the sensitivity of organic energetic materials to detonation initiation. As a science and engineering community we are still far away from having a comprehensive molecular detonation initiation theory in a widely agreed upon form. However, recent advances in experimental and theoretical methods allow for a constructive and rigorous approach to design and test the theory or at least some of its fundamental building blocks. In this review, we analyzed a set of select experimental and theoretical articles, which were augmented by our own first principles modeling and simulations, to reveal new trends in energetic materials and to refine known existing correlations between their structures, properties, and functions. Our consideration is intentionally limited to the processes of thermally stimulated chemical reactions at the earliest stage of decomposition of molecules and materials containing defects.

Keywords: sensitivity; PETN; HMX; TATB; DADNE; BNFF

1. Introduction

While detonation phenomena [1–6] were first observed a long time ago, a consistent microscale theory of detonation initiation does not yet exist [7,8]. Despite the relative maturity of the fields of shock wave physics [9,10] and chemistry of materials [11,12], detailed knowledge of the factors that govern the sensitivity of materials to the initiation of chemistry triggered by an external perturbation [13–16] has yet to be obtained, and fundamental understanding of underlying processes have yet to be established. These uncertainties hamper both the development of novel materials with tailored properties and advances of novel technologies to improve quality of life in modern society.

To be useful, high energy density materials, which possess a lot of energy that can be released upon mild external stimuli, should meet specific requirements, such as ease of synthesis, cost-efficiency, high performance, stability, and reliable safety during handling and transportation. Among the most important, most challenging, and probably least understood criteria is the low sensitivity of energetic materials to detonation initiation, dictating that the explosive decomposition chemistry will be initiated only on demand and not accidently in response to unintended perturbation.

The initiation of detonation is a complex, multi-scale process. The persistent mystery surrounding this process has inspired an exhaustive search for a primary parameter that would elucidate the intricacies of initiation sensitivity. The most notable among these attempts establish a connection between the material's sensitivity and its electronic structure [17], the band gap dynamics [18–21], the energies of relevant electronic excitations [22,23], phonon interactions [24], the energy dissipation due to plastic

deformation [25], the molecular crystal packing efficiency [26–29], and intermolecular interactions in the crystal [30–32]. Other efforts refer to correlations between the material's sensitivity and the properties of isolated molecules that comprise it; for example, the electronic charge distribution [33–36], the electronegativity [37], a combination of the quantum chemical descriptors (energies of molecular orbitals, dipole moments, and ionization potentials) [38], and selected structural parameters [39–42].

Some researchers have posited that the impact sensitivity of high explosive materials depends on the thermal stability of the molecules [43,44] rate constants [45], acid-base interactions, [46] and the oxygen balance [47]. Another set of studies employed an esoteric methodology of artificial neural networks [48,49] to link the material's sensitivity to a combination of molecular properties (the number of atoms and functional groups, bond lengths and bond angles, HOMO-LUMO energies and ionization potentials, heats of formation and bond dissociation enthalpies) [48,50].

These examples represent a fraction of publications devoted to discovering a direct correlation between sensitivity and a single descriptive parameter. It is evident, however, that a problem of such complexity requires a more elegant solution.

In this concept review, we intentionally limited our consideration to the processes of thermally stimulated chemical reactions at the earliest stage of decomposition of molecules and realistic materials containing defects. While a thermal contribution may accompany other perturbations, such as a mechanical impact or electrical shock, it is prudent to separate different effects of the materials' response to external excitations for both the simplicity and clarity of description. A notion that thermal decomposition processes play a major role in defining the sensitivity of organic energetic materials to detonation initiation was sketched in a recent review [51]. In this paper, we systematize trends in energetic materials, analyze newly suggested chemical mechanisms, and refine existing known correlations between their structures, properties, and functions. Our overarching goal is to initiate a rigorous analytic (rather than empirical) formulation of molecular initiation of detonation theory.

Here we focused on an atomistic first principles analysis of initial decomposition reactions in five classes of nitro energetic crystals, with a general formula of $C_aH_bN_cO_d$, we address several fundamental issues: (i) the molecular properties, while providing a useful insight into material's chemistry, are insufficient due to the lack of intermolecular interactions; (ii) the realistic simulations should take into account the morphology of crystals and defects; and (iii) the initiation chemistry is defined by the interplay of co-existing reactions that strongly depend upon the chemical composition of the material and its structural arrangement. We report here an analytical review to compare two traditional high explosives, nitro ester pentaerythritol tetranitrate (PETN, $C_5H_8N_4O_{12}$) and nitramine cyclotetramethylene-tetranitramine (HMX, $C_4H_8N_8O_8$) with C-nitro compounds, triamino-trinitrobenzene (TATB, $C_6H_6N_6O_6$) and experimental explosive diamino-dinitroethene (DADNE, $C_2H_4N_4O_4$), which recently gained popularity, and bis-(nitrofurazano)-furoxane (BNFF, $C_6N_8O_8$), a novel promising heterocyclic energetic material (Figure 1). A large set of experimental and theoretical data found in literature is augmented by our own calculations of chemical reactions in the organic molecules and the corresponding materials containing defects. We used only select, most relevant published articles for the analysis and illustrations and hence some papers, which are also relevant to this review, were not included in our consideration.
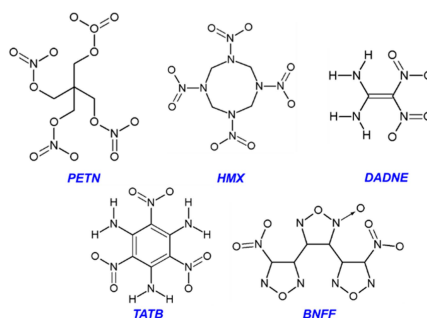

Figure 1. Schematic of PETN, HMX, DADNE, TATB, and BNFF molecular structures.

2. Computational Details

Our quantum-chemical calculations were performed using the approach [51–55] that links density functional theory (DFT) [56,57], variational transition state theory (TST), and *ab initio* chemical kinetics with a realistic description of molecules and defect containing crystals.

2.1. Gas-Phase Calculations

Modeling of gas-phase reactions is an essential and necessary part in all studies of thermally induced decomposition of nitro compounds. Modern algorithms and methods implemented in software packages allow us to obtain accurate data on geometry and vibrational structures of reagents, intermediates, products, and transitions states, model reaction pathways, calculate activation barriers, reaction energies, and pre-exponential factors. These factors provide a solid background for discussion of the competition between chemical reaction mechanisms.

Chemical reactions in the gas-phase were modeled using DFT in the GGA approximation with the PBE functional [58] and refined with hybrid exchange correlation-corrected PBE0 functional [59]. In our calculations, we use a set of available hybrid functionals depending on a specific problem. For example, fragmentation pathways of TATB and BNFF molecules were additionally explored using B3LYP, which includes Becke's three parameter [60] and the Lee–Yang–Parr correlation [61] functionals. All gas-phase calculations were performed using the split-valence double-zeta 6-31+G(2df,p) basis set as implemented in GAUSSIAN09 code [62]. Vibrational frequencies were calculated for relevant atomistic configurations to distinguish energy minima and transition states and to determine corresponding zero-point energy (ZPE) corrections. The stationary points corresponding to the energy minimum were positively identified by having no imaginary frequencies, and the transition states were confirmed to have exactly one imaginary frequency. An intrinsic reaction coordinate analysis was carried out by using the Hessian-based Predictor-Corrector integrator algorithm [63,64] for each transition state.

2.2. Periodic Calculations

Periodic solid-state calculations were performed using the GGA PBE functional and PAW pseudo-potentials [65] as implemented in the plane wave VASP code [66–68]. Using an ideal bulk structure of each molecular crystal under study, test calculations for energy convergence as a function of the number of *k*-points and the kinetic energy cut-off are required. In the smallest supercells that are needed for simulations of chemical reactions, we used $2 \times 2 \times 2$ Monkhorst−Pack *k*-point mesh in modeling ideal bulk structures of crystals (e.g., PETN, β-HMX, and DADNE). The kinetic energy cut-offs range from 520 to 800 eV, depending on the material. More details of DADNE and TATB calculations are provided in Supplementary Materials.

Full relaxation of ionic positions and lattice parameters of ideal bulk structures, initially taken from experiment, was carried out using conjugate-gradient algorithm. The convergence criterion for electronic steps was set to 10^{-5} eV, and the maximum force acting on any atom was set not to exceed 0.02 eV/Å. The lattice parameters of the crystalline structures calculated using PBE level were in reasonable agreement with experiment (1%–3%) [51], which is within typical GGA accuracy.

Modeling of chemical reactions of molecular crystals containing defects (including surfaces, vacancies, voids, or dislocations) requires constructing large supercells composed out of several hundred atoms (~500–1000). The large size of supercells serves to avoid unphysical interactions between reacting molecules (products or defects) in periodically repeated cells. Surface reactions are simulated in a slab model, in which the supercell consisted of a crystalline layer cut out of a molecular crystal in a certain direction. A 10–15 Å-thick vacuum layer, placed on top of the slab, also serves to eliminate artificial interactions between reaction products and surface fragments in directions normal to the surface plane. Whenever possible, we use in calculations surface structures that correspond to low-energy facets of crystals observed in experiment [69,70]. For newly designed or predicted materials, we study surfaces, which are likely to have a low energy based on a simplified theoretical analysis of their crystalline structures, symmetry, and possible slip systems.

Minimal energy paths in VASP periodic calculations were obtained with the nudged elastic band method [71]. Pre-exponential factors were calculated with conventional transition state theory [72] for the decomposition reactions that proceed through a formation of a transition state and with variational transition state theory [73] for the homolytic cleavage pathways.

The underestimated activation barriers, the trend characteristic of standard DFT functionals [74,75], were refined by running single point energy calculations using the hybrid PBE0 and B3LYP functionals based on the structures of reagents and transition states obtained with PBE. This technique is successfully employed to study the decomposition kinetics of nitro compounds in solid state.
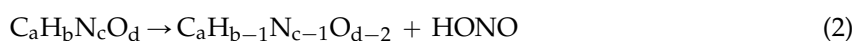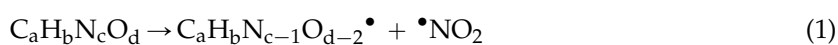
3. Results and Discussion

We analyze multiple reaction mechanisms along with their kinetics and compare various aspects of the thermal decomposition processes to reveal similarities and differences between them. These comparisons include (a) activation barriers and reaction rates of competing reactions; (b) several classes of nitro compounds; (c) molecules and crystals; (d) ideal crystals and materials containing defects; and (e) functional groups and their structural placements in the molecule. There is an important difference in chemical bonding of nitro groups to the core of the molecule. In nitrate esters, NO_2 is connected to an oxygen atom ($R–O–NO_2$), in nitramines, —to a nitrogen atom ($R–N–NO_2$), and in C-nitro explosives, —to a carbon atom ($R–C–NO_2$). This feature is often called a critical bond the increasing strength of which is correlated with the decreasing thermal sensitivity in a series PETN > HMX > DADNE and typically attributed to the lower activation barrier of the NO_2 loss in PETN than in HMX and DADNE [43,51].

3.1. PETN

Nitrate ester PETN (Figure 2) closely related to nitroglycerin is known for its dual use as a medication and a high explosive. The most stable of the nitrate esters, PETN is the most sensitive secondary high explosive in its class, and hence it is often called a benchmark compound [76,77] that classifies all materials, with the sensitivity higher than PETN, as primary explosives.

Commonly registered products of PETN decomposition are CO, CO_2, NO, N_2O, CH_2O, HCN, HNCO, and most researchers agree that the initial decomposition step is the $O-NO_2$ bond homolysis [78]. Reported experimental activation energies, E_a, of PETN decomposition are largely scattered, ranging from 30 to 70 kcal/mol [79–86]. Potential ground state decomposition mechanisms of PETN were recently scrupulously explored [87]. To avoid repetitions, we will include only two mechanisms that are most important for the initiation stage (Equations (1) and (2)).

The homolytic cleavage of the $O-NO_2$ bond (Equation (1)) is found to be the most kinetically and energetically favorable decomposition channel of the PETN molecule [88] and the (101) and (110) PETN surfaces [87]. The calculated BDE (~35 kcal/mol, Table 1) is in good agreement with the differential scanning calorimetry (DSC) measurement of 32.6 kcal/mol [86] and with a range of earlier experimental studies, 35.0 [85]–39.5 [82,89]. The elimination of the nitrous acid (HONO) (Equation (2)) is also considered a possible decomposition channel for nitro compounds containing a hydrogen atom in the β-position relative to a nitro group. This mechanism requires a slightly higher (~41 kcal/mol, Table 1) energy than the $O-NO_2$ bond scission, though the obtained activation barrier falls in the experimental range and is in general agreement with other theoretical results, 36–39 kcal/mol [88]. The HONO elimination is a much slower reaction than the NO_2 loss (Figure 3a,b) due to the low pre-exponential factor (~13, Table 1).

$$C_aH_bN_cO_d \rightarrow C_aH_bN_{c-1}O_{d-2}{}^\bullet + {}^\bullet NO_2 \tag{1}$$

$$C_aH_bN_cO_d \rightarrow C_aH_{b-1}N_{c-1}O_{d-2} + HONO \tag{2}$$

Extrapolating these findings to other nitrate esters, we can draw an important conclusion that the earliest stages of the initiation chemistry are defined by the relationship of the fast endothermic NO_2 loss reaction and the slow exothermic HONO elimination reaction. Note, the activation barrier for

the molecular gas-phase decomposition (~35 kcal/mol) almost coincides with that of the (101) surface decomposition (Table 1).
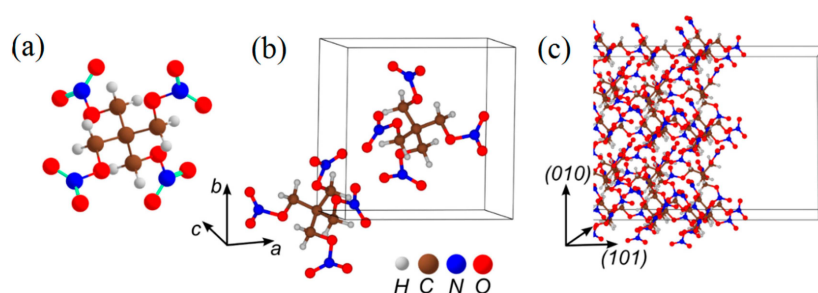

Figure 2. The structure of (**a**) the PETN molecule; (**b**) the PETN crystal; and (**c**) the model supercell representing the (101) PETN surface.

Table 1. The calculated activation barriers E (kcal/mol), zero-point-energy corrected barriers E_{ZPE} (kcal/mol), and pre-exponential factors, log (A, s^{-1}) of thermal decomposition of PETN, HMX, DADNE, TATB, and BNFF.

	Reaction		Isolated Molecule			(*mnl*) Crystal Surface		
			E	E_{ZPE}	log A	E	E_{ZPE}	log A
	PETN ($C_5H_8N_4O_{12}$)					*(101)*		
I	NO$_2^\bullet$ loss		41.8 (41.8) [a]	36.6 [34.9] b	17.5	40.0 (40.0)	35.3	17.8
II	HONO		33.6 (−18.6)	28.8 [40.5]	13.4	34.6 (−10.4)	29.5 [40.9]	14.2
	β-HMX ($C_4H_8N_8O_8$)					*(100)*		
I	NO$_2^\bullet$ loss		44.8 (44.8)	40.2 [40.9]	18.3	40.1 (40.1)	37.4	17.3
II	HONO		40.4 (−2.4)	35.8 [47.1]	13.4	41.0 (−3.2)	38.1 [47.7]	14.8
	δ-HMX ($C_4H_8N_8O_8$)					*Polar (001)*		
I	NO$_2^\bullet$ loss charge state [0] [b]		45.1 (45.1)	40.3 [41.5]	18.4	-		
	[+] [c]		12.7 (−24.3)	- [10.1]	13.4	~20.7 (−6.0)		
	[−] [c]		17.0 (17.0)	- [15.4]	-	~20.1 (20.1)		
II	HONO [0] [b]		38.0 (0.7)	33.3 [44.1]	13.3	-		
	[+] [c]		12.7 (−13.6)	- [10.1]	13.4	~20.7 (12.9)		
	DADNE ($C_2H_4N_4O_4$)					*(010)*		
I	NO$_2^\bullet$ loss		69.1 (69.1)	65.4 [68.6]	19.0	66.4 (66.4)	62.3	19.0
II	CONO		54.3 (−1.0)	52.1 [61.5]	13.5	55.3 (0.1)	52.6 [64.6]	13.8
III	1 CH$_2$N$_2$ loss (step1)		49.0 (14.7)	45.5 [49.4]	14.3	57.3 (35.2)	53.3 [62.2]	14.0
	2 CH$_2$N$_2$ loss (step2)		34.0 (14.4)	32.1 [34.4]	14.9	56.5 (38.8)	53.4 [60.7]	15.4
	3 CH$_2$N$_2$ loss (step3)		44.9 (34.6)	41.0 [47.9]	13.7	52.9 (44.5)	48.6 [58.8]	15.2
	4 NO$_2^\bullet$ loss from AIDNE		50.7 (50.7)	46.2 [47.8]	19.1	67.1 (67.1)	61.9	19.3
	TATB ($C_6H_6N_6O_6$)					*(001)*		
I	NO$_2^\bullet$ loss		74.9 (74.9)	70.7 [65.8]	18	75.0 (75.0)	71.1	19
II	CONO		54.9 (4.3)	52.5 [58.6]	13.1	54.0 (5.6)	51.5 [58.0]	13.8
III	1 H$_2$O loss (step1)		44.5 (37.5)	43.2 [42.1]	13.0	49.0 (43.0)	47.3 [46.1]	13.8
	2 H$_2$O loss (step2)		65.3 (40.9)	62.6 [68.6]	13.4	74.6 (44.5)	71.3 [74.3]	14.7
	3 H$_2$O loss (step3)		52.8 (41.7)	47.5 [58.8]	13.3	59.1 (49.5)	53.2 [65.5]	14.3
	4 HONO loss		95.4 (42.5)	91.3 [94.1]	13.4	-	-	-
	BNFF ($C_6N_8O_8$)					*(001)*		
I	NO$_2^\bullet$ loss		63.2 (63.2)	59.3 [56.2]	17.9	60.1 (60.1)	56.2	18.4
II	CONO		49.5 (−9.5)	47.2 [54.3]	13.4	49.1 (−11.0)	46.8 [51.4]	13.3
III	RC CN$_2$O$_3$		48.7 (36.4)	45.7 [50.5]	15.2	48.0 (31.7)	45.1 [49.4]	15.5
IV	RC CN$_2$O$_2$		47.1 (36.6)	44.0 [48.9]	16.3	44.2 (31.2)	41.4 [45.8]	15.4

[a] The corresponding reaction energies are shown in parentheses; [b] Activation barriers and reaction energies obtained with hybrid PBE0 (for PETN, HMX, and DADNE) and B3LYP (for BNFF) functionals are shown in square brackets; [c] Activation barriers and reaction energies for decomposition reactions of ion radicals were obtained using M06 functional.
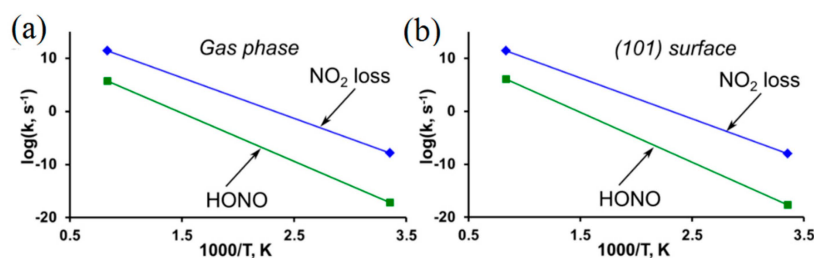
Figure 3. Reaction rates are displayed for the decomposition of PETN (**a**) in the gas phase and (**b**) on the (101) surface.

3.2. β-HMX

Nitramine HMX ($C_4H_8N_8O_8$, Figure 4a–c) [90], closely relevant to cyclotrimethylene-trinitramine (RDX, $C_3H_4N_4O_4$), is a conventional, widely used explosive and serves as a vivid representative of the nitramine class of energetics.

The main products of thermal decomposition of HMX at ambient and low pressure are CH_2O, N_2O, HCN, HONO and NO_2. As the heating rate and temperature increase, HCN and NO_2 dominate and CH_2O and N_2O play a lesser role [91]. The DSC and TGA measurements [92] of the HMX decomposition suggested that the activation barrier, E_a, falls in the range from 33.7 to 46.6 kcal/mol and the estimated pre-exponential factor log A is between 11 and 17 (s^{-1}). A logically justified and data-supported explanation to the previously reported unusually wide range of data (from 13 to 67 kcal/mol) [93,94] was developed only recently [52,53,95,96].

Similarly to nitrate esters, the homolytic NO_2 loss (Equation (1)) is the most favorable pathway of the thermal decomposition of β-HMX in the gaseous phase [97] and solid state [53,55] (Figure 5a,b). The calculated energy of the $N-NO_2$ homolysis of the isolated molecule (~41 kcal/mol, Table 1) falls in the interval of 32.1 to 52.9 kcal/mol reported for the gaseous phase [93], and is in reasonable agreement with the experimental activation energies of 38.0 [98], 39.6 [99] and 46.2 [100] kcal/mol. The cleavage of $N-NO_2$ in the HMX molecule placed on the (100) surface requires slightly lower (~37 kcal/mol, Table 1) energy than the bond dissociation of the isolated molecule (~41 kcal/mol). The activation barrier of the HONO elimination from β-HMX (~47 kcal/mol) is higher for both the gas and the surface decompositions than the corresponding cases of the $N-NO_2$ homolysis. Notably, the HONO elimination exhibits the similar barriers in the molecule and the surfaces, meaning that this is an essentially intramolecular dissociation mechanism, which is barely affected by intermolecular interactions. In addition, the HONO is a noticeably slower reaction than the $N-NO_2$ homolysis in both gaseous phase and on the (100) surface (Figure 5a,b) due to the lower pre-exponential factor and higher activation barrier (Table 1).
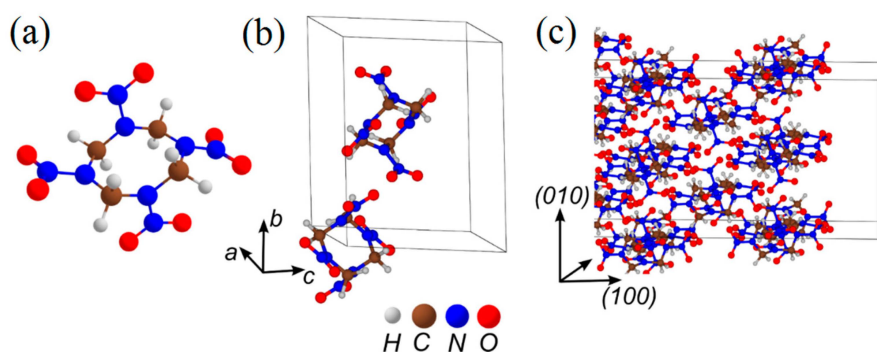

Figure 4. The structure of (**a**) an HMX molecule; (**b**) an HMX ideal crystal; and (**c**) a model supercell fragment of the (100) HMX surface.
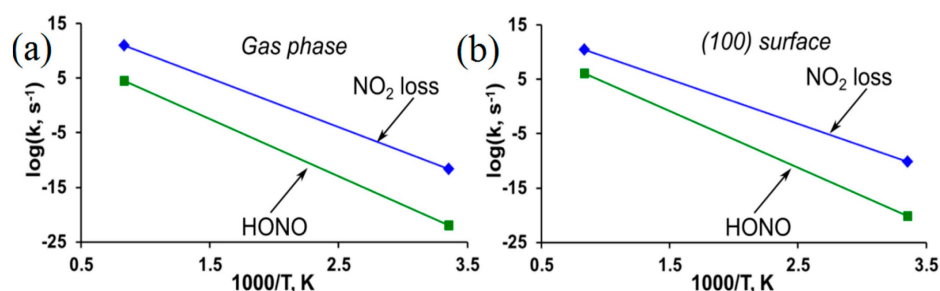
Figure 5. Reaction rates are displayed for the decomposition of β-HMX (**a**) in the gas phase and (**b**) on the (100) surface.

3.3. δ-HMX

The δ-HMX-based materials are widely used as solid fuels for rocket and space ship engines. In laboratories, δ-HMX crystals [101] (Figure 6a–c) and composites are studied due to their significantly higher sensitivity and higher burn rates than those of β-HMX [102]. The δ-HMX phase crystals are usually obtained from β-HMX phase samples by heating them above 160 °C and stimulating the β→δ phase transition [103–105]. In attempts to explain the differences in reactivity of two phases, the high sensitivity of the δ-phase (in comparison to the β-phase) was attributed to a growing number of voids during the phase transformation [106–109] and changes of the molecular structure [110,111] of the material.

Experimental measurements of δ-HMX thermal decomposition are largely lacking with an exception of two studies [112,113] that reported the activation barrier of 34.4 kcal/mol and the pre-exponential factor of log (A, s^{-1}) = 15.3.

A comparative analysis of thermal decomposition reactions of the δ-HMX molecule (boat conformation, Figure 6a) and the β-HMX (chair conformation, Figure 4a) indicated no difference in dissociation mechanisms and kinetics (Table 1) [53–55,95,96]. Thus, the changes of the molecular structure are ruled out as a possible reason for differences in sensitivities. The homolytic cleavage of the N-NO$_2$ bond Equation (1) remains the predominant decomposition pathway in both phases and requires similar energies, 41.5 kcal/mol in δ-HMX and 40.9 kcal/mol in β-HMX (Table 1). Also in both δ-HMX and β-HMX, the HONO elimination Equation (2), will unlikely compete with the NO$_2$ loss due to a high activation barrier (44.1 kcal/mol, Table 1) and a low pre-exponential factor (log(A, s^{-1}) = 13.3, Table 1).

Only simulations of HMX containing defects (ion radicals, charge transfer, and HMX surfaces) made an important reveal. It was shown that the polar (001) δ-HMX surface decomposes quite differently than any nonpolar β-HMX surface. An electric field, generated by the molecular dipoles, induces a charge transfer to form positively and negatively charged surfaces (Figure 6c). Such a charge separation creates favorable conditions for initiation of a fast reaction [51,96] thus imposing a crucial effect on thermal stability of δ-HMX. The β-HMX crystals do not have any polar surfaces and hence they do not suffer from polarization-induced instability.

Speaking in terms of activation barriers, the decomposition of δ-HMX on the positively charged surface reminds the decomposition of a radical cation (Figure 7). The NO$_2$ loss and HONO elimination on the positively charged δ-HMX surface requires 20.7 kcal/mol and proceeds via the δ-HMX *aci*-isomer formation (*I*, Figure 7). The N-NO$_2$ homolysis on the negatively charged surface requires 20.1 kcal/mol (Equation (3), Table 1) and mimics the process in the δ-HMX radical anion (17.0 kcal/mol, Table 1):

$$C_4H_8N_8O_8{}^{\bullet -} \rightarrow C_4H_8N_7O_6{}^- + {}^{\bullet}NO_2 \tag{3}$$

Interestingly, the obtained activation barriers for the δ-HMX surfaces (and also for ion radicals) are dramatically lower that these for the corresponding reactions on nonpolar β-HMX surfaces.

It is tempting to associate these low energies and fast kinetics with rather high sensitivity of δ-HMX to thermal initiation. Two important implications immediately follow from this knowledge. The activation barriers and hence the sensitivity of polar δ-HMX are comparable to those of primary explosives, metal azides, SrN_6 (20 kcal/mol), CuN_3 (27 kcal/mol), PbN_6 (29 kcal/mol) and AgN_3 (32 kcal/mol) [114]. Further, the wide range of experimental activation barriers reported for HMX can be attributed to various crystallographic phases, including both β- and δ-HMX. With polar δ-HMX facets requiring appreciably lower activation energy than β-HMX facets, an unusually large scattering of activation barriers in the overall thermal initiation should be expected.
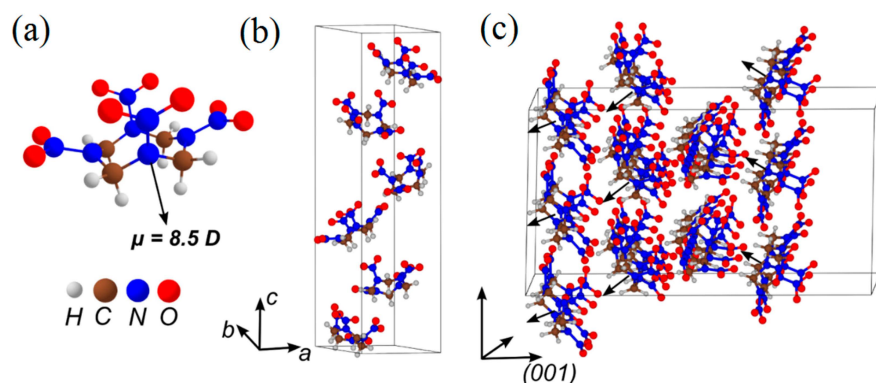
Figure 6. The structure of (**a**) a boat conformer of δ-HMX molecule with the dipole moment μ; (**b**) an δ-HMX ideal crystal; and (**c**) a model supercell fragment of the (001) δ-HMX surface.
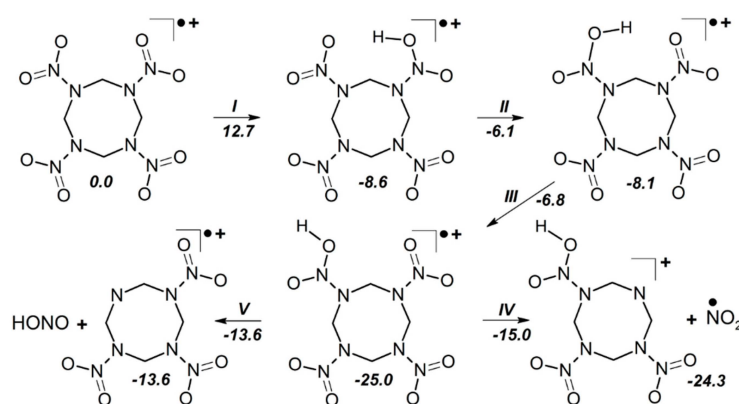

Figure 7. A schematic representation of fragmentation pathways of δ-HMX radical cation.

3.4. DADNE

Details of synthesis [115], structure [116] and physico-chemical properties [117] of DADNE (Figure 8) were reported in 1998 when the material had a promise to combine two important properties, high performance and low sensitivity. Structurally, DADNE ($C_2H_4N_4O_4$) is often compared to HMX ($C_4H_8N_8O_8$), RDX ($C_3H_6N_6O_6$), and TATB ($C_6H_6N_6O_6$). The high performance of DADNE, similar to HMX and RDX was attributed to the same stoichiometry (the DADNE molecule represents ½ of an HMX molecule and 2/3 of an RDX molecule). On the other hand, the critical chemical bond of DADNE, C-NO_2, reminding TATB, inspired high hopes for low sensitivity, analogous to TATB. The molecular configuration of DADNE (Figure 8a) can be described as a push-pull ethylene with two donor amino groups ("head") and two withdrawing nitro groups ("tail"). In the crystal (Figure 8b), polar DADNE molecules are packed "head-to-tail" forming wave-shaped layers with linear intermolecular hydrogen bonding within the layers and weak van der Waals interactions between the layers [116].
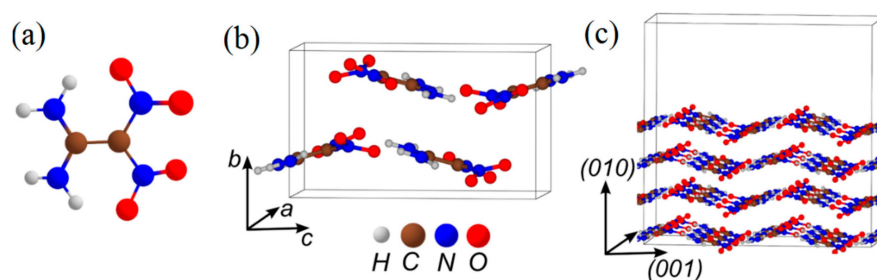
Figure 8. The structure of (**a**) a DADNE molecule; (**b**) a DADNE ideal crystal; and (**c**) a model supercell fragment of the (010) surface.

Earlier results of the drop hammer test ($h_{50\%}$ = 126–159 cm) pointed toward significantly lower impact sensitivity of DADNE relative to nitramine RDX ($h_{50\%}$ = 38 cm) [118]. The reported activation energy of the thermal decomposition of DADNE (58 kcal/mol) [117] is closer to nitroarenes (>60 kcal/mol) than nitroesters (~35 kcal/mol) or nitamines (~40–45 kcal/mol), which also points towards higher thermal stability of the material. Hence, it is not surprising that DADNE became an object of many experimental and theoretical studies. Despite the extensive effort of researchers, many questions regarding stability of DADNE remain unanswered.

Experimental measurements of the activation energy for DADNE decomposition that became available over last two decades appear scattered in the range of 45–80 kcal/mol [117,119,120]. The CO_2, HCN, N_2O, NO_2, HOCN, H_2O, and NO species were registered among decomposition products of DADNE [117,119].

Ordinarily, the $C-NO_2$ bond homolysis [121,122] (path *I*, Figure 9) and NO loss proceeding via CONO isomerization [122–124] (path *II*, Figure 9) have been considered the main favorable mechanisms of DADNE thermal decomposition. In contrast to a traditional view and earlier conclusions, recent theoretical studies [125,126] proposed yet another possible decomposition mechanism with even lower activation barrier (~45 kcal/mol) proceeding via an enamino-imino isomerization (path *III*, Figure 9) in the gas phase. We rigorously reevaluated conventional reactions and tested newly proposed mechanisms for DADNE decomposition.
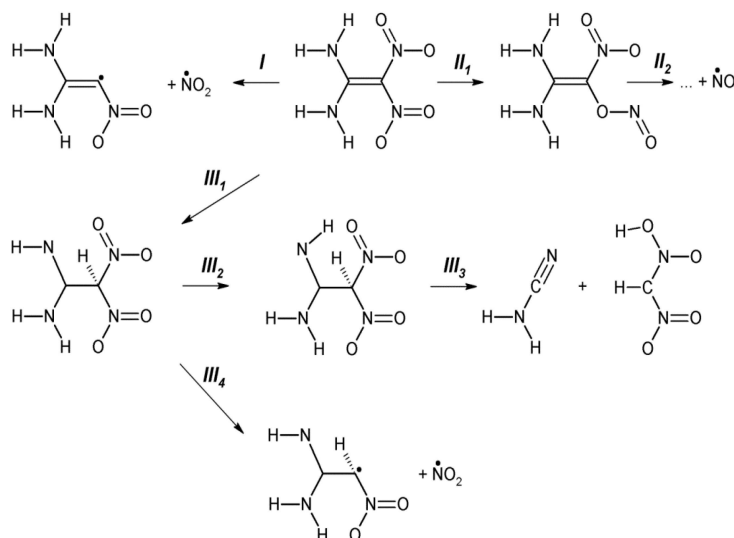

Figure 9. A schematic representation of DADNE fragmentation pathways.

Our calculations confirm that the enamine-imine isomerization (path III_1, Figure 9), leading to a formation of 1-amino-1-imino-2,2-dinitroethane (AIDNE), has the lowest activation barrier

(49.4 kcal/mol, Table 1) among potential primary decomposition steps in the gas phase, the NO_2 loss (68.6 kcal/mol) and CONO isomerization (61.5 kcal/mol). There are two possible channels of further decomposition of AIDNE. The first channel involves a rotation of the NH fragment about the C-N bond (path *III*$_2$, Figure 9) and the subsequent CH_2N_2 elimination via the C-C bond cleavage (path *III*$_3$, Figure 9). Both reaction steps *III*$_2$ and *III*$_3$ (34.4 and 37.4 kcal/mol, Figure 9) require a lower energy than the primary enamine-imine isomerization (Table 1). The second possible channel of AIDNE proceeds via the homolytic C-NO_2 bond cleavage (path *III*$_4$, Figure 9) and requires overall 47.8 kcal/mol (Table 1).

The calculated reaction rates (Figure 10a) indicate that the CH_2N_2 elimination (path *III*$_1 \rightarrow III_3$, Figure 9) and the NO_2 loss from AIDNE (path *III*$_1 \rightarrow III_4$, Figure 9) are predominant decomposition pathways of DADNE in the gas phase, and the primary enamine-imine isomerization (path *III*$_1$, Figure 9) should be considered as the rate limiting step.
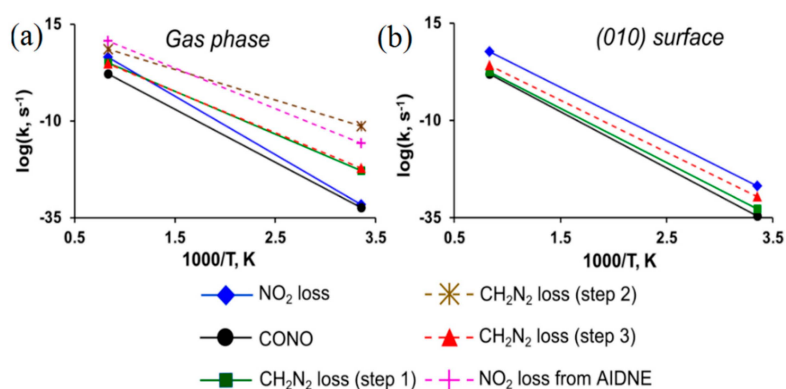

Figure 10. Reaction rates of DADNE decomposition (**a**) in the gas phase and (**b**) on the (010) surface.

Further, we simulated the same decomposition mechanisms on DADNE crystals. The homolytic C-NO_2 bond cleavage (path *I*, Figure 9) proceeding on the (010) surface (Figure 8c) requires slightly lower energy than that in the gas phase, whereas the CONO isomerization (path *II*, Figure 9) on the (010) surface has slightly higher activation barrier than that in the isolated molecule (Table 1). The strongest effect the (010) surface makes on kinetics of fragmentation channels associated with the enamine-imine isomerization (path *III*, Table 1). The activation barriers of the enamine-imine isomerization (62.2 kcal/mol, path *III*$_1$, Table 1), rotation of the NH fragment about the C-N bond (60.7 kcal/mol, path *III*$_2$, Figure 9) and subsequent CH_2N_2 elimination (58.8 kcal/mol, path *III*$_3$, Figure 9) are 12–25 kcal/mol higher that the gas-phase reactions (49.4, 34.4 and 47.9 kcal/mol, respectively, Table 1). The NO_2 loss from AIDNE proceeding on the (010) surface (path *III*$_4$, Figure 9) also requires ~16 kcal/mol higher energy (61.9 kcal/mol, Table 1) than in the gas phase (46.2 kcal/mol, Table 1). An increase of activation energies is also reflected in the reaction kinetics. As a result, the enamine-imine isomerization proceeds on the (010) surface (path *III*$_1$, Table 1) at lower rates than the NO_2 loss (Figure 10b). Therefore, we conclude that the homolytic C-NO_2 bond cleavage remains the predominant decomposition channel of DADNE crystals on the (010) surface.

The thermal decomposition mechanism and kinetics of DADNE are strongly dependent upon the crystal structure. As a result DADNE will likely to decompose in the solid state via the homolytic NO_2 loss, though several kinetically more favorable fragmentation channels were proposed for gaseous phase. This example with DADNE demonstrates that explicit modeling of the solid state decomposition processes is required for analyzing materials sensitivity and molecular calculations alone do not provide sufficient and reliable information.

3.5. TATB

TATB (Figure 11) is the benchmark high density energy material that is characterized by the lowest achieved sensitivity against impact ($h_{50\%} > 320$ cm) [127] and against thermal decomposition

(E$_a$ = 59–68 kcal/mol) [128,129]. There are several theoretical studies reporting the energies of activation barriers for the C-NO$_2$ bond scission (64–77 kcal/mol) [44,130–132] and CONO isomerization (55 kcal/mol) [124]. Results of some studies also suggest that an elimination of water may be the predominant channel for thermal decomposition of TATB [130]. Surprisingly, however, a detailed theoretical study of thermal decomposition of TATB that analyses both molecular and crystalline processes based on quantum chemical methods is still lacking. Therefore, we simulated several viable fragmentation mechanisms of TATB in the gas phase and solid state aimed at obtaining kinetic data and performing a more comprehensive analysis of thermal sensitivity of this material than was available up to now.
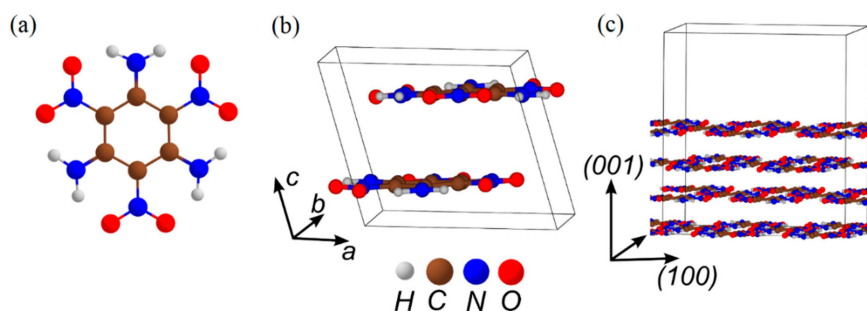

Figure 11. The structure of (**a**) a TATB molecule; (**b**) a TATB ideal crystal; and (**c**) a model supercell fragment of the (001) surface.

We found that the rupture of the C-NO$_2$ bond (path *I*, Figure 12) requires 65–70 kcal/mol in the gas phase (Table 1). The CONO isomerization (path *II*, Figure 12) is a less demanding process with the activation barrier of 58.6 kcal/mol (Table 1). An alternative mechanism of water elimination from TATB (path *III*$_1$–*III*$_3$, Figure 12) is a stepwise process. The primary step (path *III*$_1$, Figure 12) involves a formation of the *aci*-isomer of TATB and requires relatively low energy of 42.1 kcal/mol (Table 1). A rotation of the HONO fragment about the C-N bond (path *III*$_2$, Figure 12) proceeds during the second step with the overall activation barrier of 68.6 kcal/mol (Table 1). Finally, an elimination of the H$_2$O molecule costs 58.8 kcal/mol (Table 1). The stepwise elimination of HONO from TATB (path *III*$_1$-*III*$_4$, Figure 12) has the highest activation barrier of 94.1 kcal/mol (Table 1).

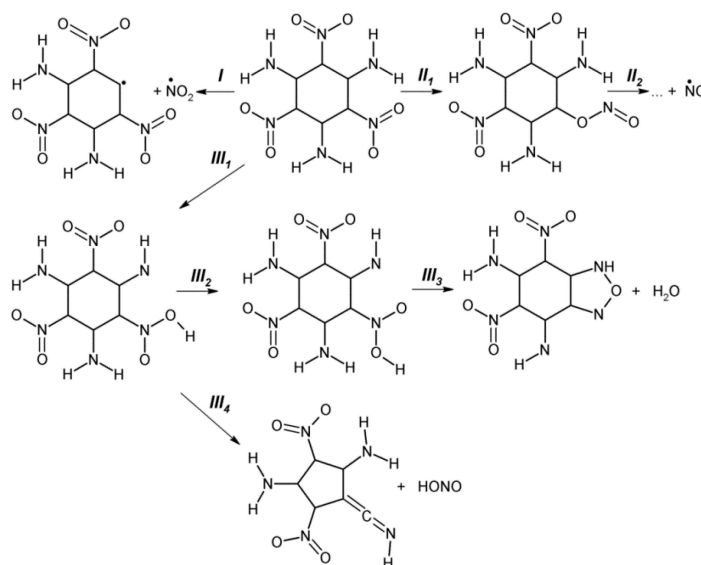**Figure 12.** A schematic representation of TATB fragmentation.

Pre-exponential factors and reaction rates depicted in Figure 13 show that the C-NO$_2$ fission is the dominating decomposition pathway in the gas phase at high temperatures (T > 400 K). With the lower activation barrier (by ~8 kcal/mol, Table 1), the CONO isomerization will be the fastest reaction at low temperatures due to relatively low pre-exponential factor (Table 1). Elimination of the water molecule will unlikely compete with these two reactions due to the high overall activation barrier of the rate limiting stage associated with the rotation of the HONO fragment (68.6 kcal/mol, path *III$_2$*, Figure 12) and the moderate pre-exponential factor (log(A, s^{-1}) = 13.4, Table 1). The HONO loss from TATB (94.1 kcal/mol, path *III$_1$-III$_4$*, Figure 12) is the slowest reaction due to its significantly high activation barrier and relatively low pre-exponential factor (log(A, s^{-1}) = 13.4, Table 1). This leads us to exclude this mechanism from further consideration in simulations of thermal decomposition pathways of solid state TATB.
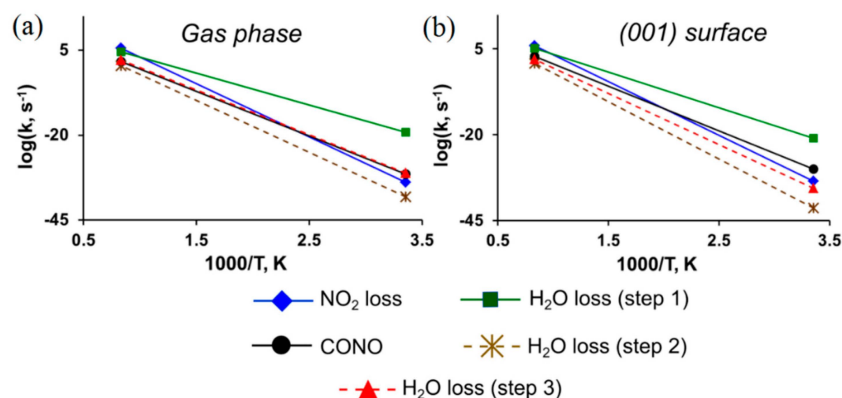

Figure 13. Reaction rates of TATB decomposition (**a**) in the gaseous phase and (**b**) on the (001) surface.

The decomposition of TATB on the (001) surface obeys the same general trends as the process in the gas-phase. All reactions proceeding on the (001) surface have slightly higher activation energies except the CONO isomerization (Table 1). The pre-exponential factors collected in Table 1 and reaction rates depicted in Figure 13 reveal two main competing channels with the NO$_2$ loss being the dominating decomposition pathway at T > 500 K and the CONO isomerization dominating at low temperatures. Elimination of water from TATB will unlikely compete with the two channels (Figure 13) due to the high overall activation barriers and moderate pre-exponential factors of secondary reactions (Table 1) associated with the rotation of the HONO fragment in the *aci*-form of TATB (paths *III$_2$*, Figure 12) and H$_2$O loss (paths *III$_3$*, Figure 12). Interestingly, our periodic calculations found that the activation barrier of the primary step, the intramolecular hydrogen transfer, and the formation of *aci*-isomer of TATB (paths *III$_1$*, Figure 12), proceeding on (001) surface is 46.1 kcal/mol (Table 1), which is even lower than the earlier estimates of 76.1 kcal/mol [133] obtained using an embedded cluster model. Despite this, the water loss reaction cannot be considered the primary initiation reaction of TATB decomposition.

In general, the calculated here energy of the C-NO$_2$ bond scission (65–71 kcal/mol, Table 1) and the activation barrier of the CONO rearrangement (58 kcal/mol, Table 1) are in good agreement with the range of experimentally measured activation energies 59–68 kcal/mol [128,129].

3.6. BNFF

BNFF (Figure 14) is a recently developed, attractive heterocyclic energetic compound with good thermal stability, low melting point (110 °C), high density (1.937 g/cm^3), and moderate sensitivity to various insults [134]. BNFF belongs to C-nitro compounds and is predicted to possess a low sensitivity due to the C-NO$_2$ bond, heterocyclic molecular structure, and densely packed molecular crystal arrangement (Figure 14a–c). In our study, BNFF represents the whole class of heterocyclic C-nitro explosive materials. The idea here is to explore whether such an arrangement of the molecule and the

crystal will gain additional stability against a thermal perturbation and thus improve (*i.e.*, lower) the sensitivity of the material to initiation of detonation.
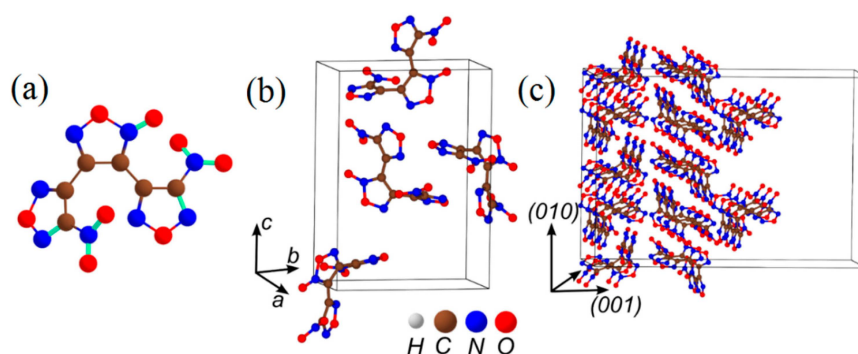

Figure 14. The structure of (**a**) a BNFF molecule; (**b**) a BNFF ideal crystal, and (**c**) a model supercell fragment of the (001) surface.

The calculated energy of the homolytic $C-NO_2$ bond cleavage in BNFF (path *I*, Figure 15) is 56–59 kcal/mol (depending on the DFT functional, Table 1), which is comparable with the strength of the $C-NO_2$ bond in DADNE and TATB and notably higher than the $X-NO_2$ bond fissions in nitrate esters and nitramines (Table 1). The further investigation of alternative mechanisms revealed the reaction pathways, which can be activated with even lower energies than the $C-NO_2$ homolysis. For example, the CONO isomerization (54.3 kcal/mol path *II*, Figure 15) requires a somewhat lower activation barrier (by 1–3 kcal/mol, Table 1) than the $C-NO_2$ bond fission (56.2 kcal/mol, Table 1), and being an exothermic reaction, releases ~10 kcal/mol of heat (Table 1). However, Figure 16a shows that the CONO isomerization is slower than the NO_2 loss due to a lower pre-exponential factor (Table 1). The elimination of the CN_2O_3 molecule via the outer oxadiazol ring cleavage (path *III*, Figure 15) in BNFF requires 50.5 kcal/mol (Table 1). Another possible pathway for the opening of the outer heterocyclic rings (path *IV*, Figure 15) proceeds via elimination of CN_2O_2 and demands even lower energy (48.9 kcal/mol, Table 1) and hence it will dominate during gas-phase decomposition at T < 500 K (Figure 16a).
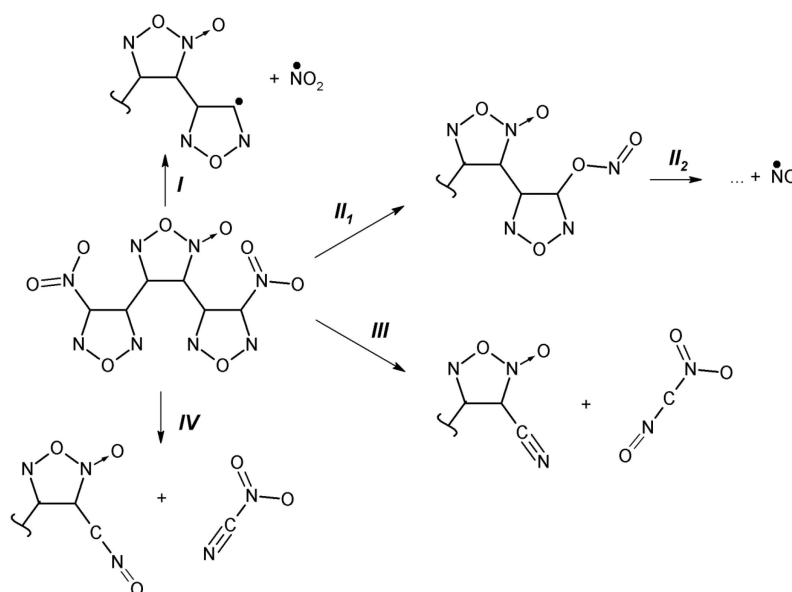

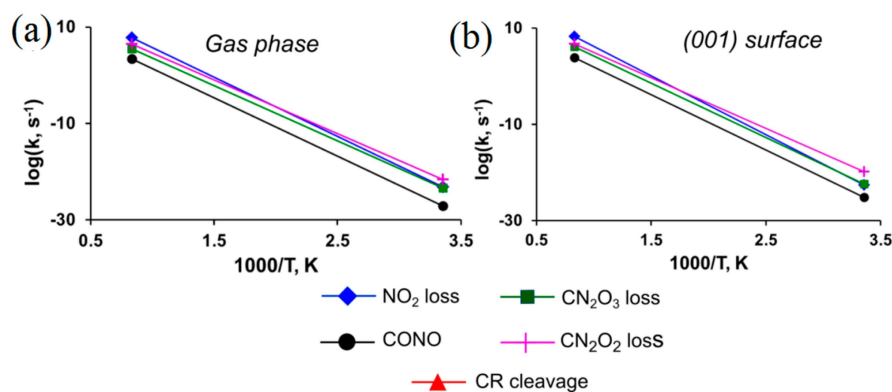**Figure 15.** Schematic representation of BNFF fragmentation.

Figure 16. Reaction rates of BNFF decomposition (**a**) in the gas phase and (**b**) on (001) surface.

The elimination of CN_2O_2 via concerted breaking of the outer oxadiazol ring remains the predominant decomposition channel on the (001) BNFF surface. The calculated activation barriers of the outer ring cleavage of BNFF on the (001) surface (45.8 kcal/mol, Table 1) seems to agree well with the experimental estimate of 42.3 kcal/mol [135]. The calculated pre-exponential factors ($\log(A, s^{-1})$ ~15, Table 1) are also consistent with the experimental value ($\log(A, s^{-1}) = 13.68$) [135]. The scission of the $C-NO_2$ bond in BNFF on the (001) surface, although requires 3.1 kcal/mol lower energy than that in the gas-phase (Table 1), is still significantly (~10 kcal/mol, Table 1) higher than the activation barrier of the CN_2O_2 loss. As the result, the CN_2O_2 elimination will dominate the decomposition on the (001) surface at T < 650 K (Figure 16b), whereas the $C-NO_2$ loss will dominate at high temperatures.

4. Conclusions

This review aimed at presenting a conceptual, first principles analysis of initiation of thermal decomposition reactions in several classes of organic nitro energetic crystals to instigate the development of the molecular theory of initiation of detonation. Despite existing classic macroscale theories [6,136–140] and thousands of papers published in the field of energetic materials, the fundamental understanding of the initiation of chemistry phenomena is limited to micro- and nano-scale. Consequently, significant breakthroughs may be achieved only when chemical and physical mechanisms of materials' behavior are revealed at the molecular scale.

We reviewed relevant experimental and theoretical literature and augmented the available data by our own simulations to fill the gaps or to test notions recently suggested by researchers. In order to lay groundwork for the future microscale theory, we selected a set of organic energetic materials, nitro ester PETN, nitramine HMX, and C-nitro compounds, TATB, DADNE, and BNFF. Such a set, which combined conventional explosives in use (PETN, HMX, and TATB) with experimental promising energetic materials (DADNE and BNFF), serves to reveal (or confirm and enhance) general trends in chemical decomposition, identify (or supplement and refine) meaningful correlations between structures and properties, and test some novel ideas in the field.

Our modeling of decomposition reactions in the gaseous phase and solid state showed that thermal degradation of explosives is a complex process that often involves several mechanisms triggered with similar activation barriers and progressing with close rates. It is rather unusual that only one reaction would initiate decomposition and continue to progress for a notable time, especially in crystals. One mechanism is typically dominating with another reaction or even two reactions starting somewhat later, which however can switch and become prevailing reactions at higher temperatures. For example, the homolytic loss of NO_2 will be the dominant decomposition pathway for PETN and HMX at a rather wide range of temperatures with the HONO isomerization proceeding as a slow background reaction. In the case of TATB, the $C-NO_2$ bond fission will dominate at high temperature and the CONO isomerization will proceed at higher rates at low temperatures.

The decomposition initiation is comprehensively characterized by a set of descriptors: identified chemical mechanisms, activation barriers, reaction energies, pre-exponential factors, and reactions rates. Only together they reproduce the decomposition picture and if a parameter or two are missing, the lack of data may be misleading. This finding clearly illustrates how hopeless are the attempts to find a single descriptive parameter to measure the sensitivity of materials to initiation and even the thermal decomposition of materials, which represents only one component contributing in sensitivity.

Another factor that strongly affects the decomposition kinetics is a molecular and crystalline structure of the material of interest. We found that the well-accepted correlation between the strength of the critical X-NO$_2$ bond and the sensitivity of materials, which roughly follows the series E(C-NO$_2$) > E(N-NO$_2$) > E(O-NO$_2$), is only approximately valid for some isolated molecules (but not all) and certainly it does not work for crystals. Indeed, the difference in the thermal stability of PETN (and most nitro esters) and β-HMX (and most nitramines) can be closely enough explained by a comparison of activation energies required for breaking these critical bonds. The similar approach however cannot be used for analyzing the relative thermal stabilities of HMX polymorphs, β- and δ-phases, or C-nitro compounds, DADNE, TATB and BNFF. The C-NO$_2$ bond fission reaction can be largely considered the predominant pathway for decomposition of DADNE and TATB and hence allows for a parallel comparison between these two materials. The stability of BNFF, on the other hand, is mainly determined by the fragmentation mechanisms associated with the cleavage of oxadiazole rings, which require significantly lower activation energy than the C-NO$_2$ bond cleavage. Although the ring cleavage reaction is overpowered by the C-NO$_2$ loss upon a moderate increase of temperature, the sensitivity of BNFF is higher than what is expected from desired C-nitro materials. This conclusion demonstrates that the chemical composition and the presence of functional groups are as important for defining the stabilization of molecules and materials as the details of the molecular structure and hence may serve as a useful feature for design of new materials with targeted properties and functions.

The crystalline structure and intermolecular interactions impose additional limitations on kinetics and mechanisms of the decomposition of nitro compounds. Mechanisms that may dominate the gas-phase decomposition of single molecules may be restricted or even completely suppressed in the solid state. For example, the recently proposed decomposition mechanism of DADNE via the enamino-imino isomerization followed by the elimination of either CH$_2$N$_2$ or NO$_2$ requires, indeed, a low energy in the gas-phase, which makes this reaction a feasible initiation pathway. However, once the decomposing DADNE molecule is placed on the (010) surface, the overall activation energy of this channel significantly increases due to Coulomb repulsion between neighbor molecules. This precludes DADNE from decomposition through this channel and the C-NO$_2$ bond fission becomes the main reaction in the solid-state.

Because energetic materials are densely packed, we predict that there are many other manifestations of the crystal arrangement governing the decomposition chemistry and hence the sensitivity. To mention just a few vivid illustrations, we recall the shear-strain effect in DADNE [21,124,141], the aspects of autocatalysis analyzed for DADNE and TATB [124], polarization-induced charge transfer in δ-HMX [96], enhanced optical absorption on PETN-MgO interfaces [142], and photocatalytic dissociation of PETN molecules adsorbed on F^0-centers on the α-Al$_2$O$_3$ (0001) surfaces [143]. A variety of structural and electronic defects also play a role in changing decomposition chemistry in organic molecular crystals [19,122,133,144–146]. Without a doubt, these factors have to be carefully analyzed in series of other energetic materials to confirm, refine, and generalize the trends and correlations. Advanced large-scale quantum chemical methods [147–149] may need to be involved for such studies, as recently reviewed [150], however they require serious adaptations to become useful for modeling of energetic materials. We would like to emphasize here that partnerships between experimental and theoretical groups, combinations of available methods, and the development of new multi-scale multi-physics techniques are required for studies of the physical and chemical properties of the existing materials and assisting synthesis of novel energetic materials.

Summing up, this review presents a conceptual assessment of thermal decomposition trends in energetic materials that should serve as a solid ground for building the molecular theory of detonation initiation from first principles. By analyzing a large volume of experimental and theoretical studies we would like to emphasize several conclusions and observations. (i) The molecular properties (chemical composition and mutual positions of functional groups in the molecule) define chemistry of individual molecules and therefore provide a useful insight into material's stability. However by no means conclusions made for gas-phase processes may be extrapolated to materials properties. They are insufficient due to the lack of intermolecular interactions in molecular models; (ii) The realistic quality simulations of materials should take into account the morphology of crystals and defects as they are imperative for reliable predictions and for comparison with experimental studies; (iii) In most energetic materials, the initiation chemistry is defined by the interplay of co-existing reactions that strongly depend upon the chemical composition of the material and its structural arrangement.

Author Contributions: All authors equally contributed to this review.

Conflicts of Interest: The authors declare no conflict of interest.

References

1. Berthelot, M.; Vieille, P. Sur la vitesse de propagation des phénomènes explosifs dans les gaz. *C.R. Acad. Sci.* **1881**, *93*, 18–22.

2. Mallard, E.; le Chatelier, H. Sur les vitesses de propagation de l'inflammation dans les mélanges gazeux explosifs. *C.R. Ac. Sc.* **1881**, *93*, 145–148.

3. Chapman, D.L. On the rate of explosion in gases. *Philos. Mag.* **1899**, *47*, 90–104. [CrossRef]

4. Jouguet, E. On the propagation of chemical reactions in gases. *J. Math. Pures Appl.* **1905**, *2*, 347–425.

5. Zeldovich, Y.B. On the utilization of detonative combustion energy. *Technol. Phys.* **1940**, *10*, 1453–1461.

6. Döring, W. On detonation processes in gases. *Ann. Phys.* **1943**, *43*, 421–436. [CrossRef]

7. Fickett, W.; Davis, W.C. *Detonation: Theory and experiment*; Courier Corporation: Mineola, NY, USA, 2012; p. 403.

8. Fickett, W.; Wood, W.W. Flow calculations for pulsating one-dimensional detonations. *Phys. Fluids* **1966**, *9*, 903–916. [CrossRef]

9. Bridgman, P.W. Water, in the liquid and five solid forms, under pressure. *Proc. Am. Acad. Arts Sci.* **1912**, *47*, 441–558. [CrossRef]

10. Dremin, A.N. Discoveries in detonation of molecular condensed explosives in the 20th century. *Combust. Explos. Shock Waves* **2000**, *36*, 704–715. [CrossRef]

11. Eyring, H.; Daniels, F. The decomposition of nitrogen pentoxide in inert solvents. *J. Am. Chem. Soc.* **1930**, *52*, 1472–1486. [CrossRef]

12. Eyring, H.; Daniels, F. The decomposition of nitrogen pentoxide in chemically active solvents. *J. Am. Chem. Soc.* **1930**, *52*, 1486–1492. [CrossRef]

13. Politzer, P., Murray, J.S., Eds.; Energetic materials: Part 1. Decomposition, crystal and molecular properties, and part 2. Detonation, combustion. In *Theoretical and Computational Chemistry*; Elsevier: Amsterdam, The Netherland, 2003.

14. Yan, Q.L.; Zeman, S. Theoretical evaluation of sensitivity and thermal stability for high explosives based on quantum chemistry methods: A brief review. *Int. J. Quant. Chem.* **2013**, *113*, 1049–1061. [CrossRef]

15. Chen, Z.X.; Xiao, H.M. Quantum chemistry derived criteria for impact sensitivity. *Propellants Explos. Pyrotech.* **2014**, *39*, 487–495. [CrossRef]

16. Zhang, L.; Zybin, S.V.; van Duin, A.C.T.; Goddard, W.A., III. Modeling high rate impact sensitivity of perfect RDX and HMX crystals by ReaxFF reactive dynamics. *J. Energ. Mater.* **2010**, *28*, 92–127. [CrossRef]

17. Kunz, A.B. *Ab initio* investigation of the structure and electronic properties of the energetic solids TATB and RDX. *Phys. Rev. B* **1996**, *53*, 9733–9738. [CrossRef]

18. Kuklja, M.M.; Stefanovich, E.V.; Kunz, A.B. An excitonic mechanism of detonation initiation in explosives. *J. Chem. Phys.* **2000**, *112*, 3417–3423. [CrossRef]

19. Kuklja, M.M.; Aduev, B.P.; Aluker, E.D.; Krasheninin, V.I.; Krechetov, A.G.; Mitrofanov, A.Y. The role of electronic excitations in explosive decomposition of solids. *J. Appl. Phys.* **2001**, *89*, 4156–4166. [CrossRef]

20. Kuklja, M.M.; Rashkeev, S.N. Shear-strain induced structural and electronic modifications of the molecular crystal 1,1-diamino-2,2-dinitroethylene: Slip-plane flow and band gap relaxation. *Phys. Rev. B* **2007**, *75*. [CrossRef]

21. Kuklja, M.M.; Rashkeev, S.N.; Zerilli, F.J. Shear-strain induced decomposition of 1,1-diamino-2,2-dinitroethylene. *Appl. Phys. Lett.* **2006**, *89*. [CrossRef]

22. Sharma, J.; Beard, B.C. Electronic excitations preceding shock initiation in explosives. *MRS Proc.* **1992**, *296*. [CrossRef]

23. Bernstein, E.R. On the release of stored energy from energetic materials. *Adv. Quantum Chem.* **2014**, *69*, 31–70.

24. Chen, S.; Tolbert, W.A.; Dlott, D.D. Direct measurement of ultrafast multiphonon up-pumping in high explosives. *J. Phys. Chem.* **1994**, *98*, 7759–7766. [CrossRef]

25. Coffey, C.S.; Sharma, J. Plastic deformation, energy dissipation, and initiation of crystalline explosives. *Phys. Rev. B* **1999**, *60*, 9365–9371. [CrossRef]

26. Pospíšil, M.; Vávra, P.; Concha, M.C.; Murray, J.S.; Politzer, P. Sensitivity and the available free space per molecule in the unit cell. *J. Mol. Model.* **2011**, *17*, 2569–2574. [CrossRef] [PubMed]

27. Politzer, P.; Murray, J.S. Impact sensitivity and crystal lattice compressibility/free space. *J. Mol. Model.* **2014**, *20*. [CrossRef] [PubMed]

28. Politzer, P.; Murray, J.S. Detonation performance and sensitivity: A quest for balance. *Adv. Quantum Chem.* **2014**, *69*, 1–30.

29. Zhang, C.; Wang, X.; Huang, H. π-Stacked interactions in explosive crystals: Buffers against external mechanical stimuli. *J. Am. Chem. Soc.* **2008**, *130*, 8359–8365. [CrossRef] [PubMed]

30. Brill, T.B.; Reese, C.O. Analysis of intra- and intermolecular interactions relating to the thermophysical behavior of *a*-, 6-, and *b*-octahydro-l,3,5,7-tetranltro-1,3,5,7-tetraazocine. *J. Phys. Chem.* **1980**, *84*, 1376–1380. [CrossRef]

31. Taylor, D.E. *Prediction of the Impact Sensitivity of Energetic Materials Using Symmetry Adapted Perturbation Theory*; Army Research Laboratory Technical Report: Aberdeen, MD, USA; May; 2011.

32. Jones, T. Role of inter- and intramolecular bonding on impact sensitivity. *J. Phys. Chem. A* **2012**, *116*, 11008–11014. [CrossRef] [PubMed]

33. Rice, B.M.; Hare, J.J. A quantum mechanical investigation of the relation between impact sensitivity and the charge distribution in energetic molecules. *J. Phys. Chem. A* **2002**, *106*, 1770–1783. [CrossRef]

34. Murray, J.S.; Lane, P.; Politzer, P.; Bolduc, P.R. A relationship between impact sensitivity and the electrostatic potentials at the midpoints of C-NO$_2$ bonds in nitroaromatics. *Chem. Phys. Lett.* **1990**, *168*, 135–139. [CrossRef]

35. Politzer, P.; Murray, J.S.; Seminario, J.M.; Lane, P.; Grice, M.E.; Concha, M.C. Computational characterization of energetic materials. *Comp. Theor. Chem.* **2001**, *573*, 1–10. [CrossRef]

36. Murray, J.S.; Concha, M.C.; Politzer, P. Links between surface electrostatic potentials of energetic molecules, impact sensitivities and C-NO$_2$/N-NO$_2$ bond dissociation energies. *Mol. Phys.* **2009**, *107*, 89–97. [CrossRef]

37. Mullay, J. A relationship between impact sensitivity and molecular electronegativity. *Propellants Explos. Pyrot.* **1987**, *12*, 60–63. [CrossRef]

38. Badders, N.R.; Wei, C.; Aldeeb, A.A.; Rogers, W.J.; Mannan, M.S. Predicting the impact sensitivities of polynitro compounds using quantum chemical descriptors. *J. Energ. Mater.* **2006**, *24*, 17–33. [CrossRef]

39. Politzer, P.; Murray, J.S.; Lane, P.; Sjoberg, P.; Adolph, H.G. Shock-sensitivity relationships of nitramines and nitroaliphatics. *Chem. Phys. Lett.* **1991**, *181*, 78–82. [CrossRef]

40. Keshavarz, M.H.; Pouretedal, H.R.; Semnani, A. Simple empirical method for prediction of impact sensitivity of selected class of explosives. *J. Hazard. Mater.* **2005**, *A124*, 27–33. [CrossRef] [PubMed]

41. Keshavarz, M.H. Prediction of impact sensitivity of nitroaliphatic, nitroaliphatic containing other functional groups and nitrate explosives. *J. Hazard. Mater.* **2007**, *148*, 648–652. [CrossRef] [PubMed]

42. Keshavarz, M.H.; Pouretedal, H.R. Novel correlation for predicting impact sensitivity of nitroheterocyclic energetic molecules. *J. Hazard. Mater.* **2007**, *141*, 803–807. [CrossRef] [PubMed]

43. Owens, F.J. Calculation of energy barriers for bond rupture in some energetic molecules. *Theochem. J. Mol. Struct.* **1996**, *370*, 11–16. [CrossRef]

44. Rice, B.M.; Sahu, S.; Owens, F.J. Density functional calculations of bond dissociation energies for NO_2 scission in some nitroaromatic molecules. *Theochem. J. Mol. Struct.* **2002**, *583*, 69–72. [CrossRef]

45. Mathieu, D.; Alaime, T. Predicting impact sensitivities of nitro compounds on the basis of a semi-empirical rate constant. *J. Phys. Chem. A* **2014**, *118*, 9720–9726. [CrossRef] [PubMed]

46. Koch, E.C. Acid-base interactions in energetic materials: I. the hard and soft acids and bases (HSAB) principle—Insights to reactivity and sensitivity of energetic materials. *Propellants Explos. Pyrotech.* **2005**, *30*, 5–16. [CrossRef]

47. Kamlet, M.J.; Adolph, H.G. The relationship of impact sensitivity with structure of organic high explosives. II. Polynitroaromatic explosives. *Propellants Explos.* **1979**, *4*, 30–34. [CrossRef]

48. Zhao, J.; Cheng, X.L.; He, B.; Yang, X.D. Neural networks study on the correlation between impact sensitivity and molecular structures for nitramine explosives. *Struct. Chem.* **2006**, *17*, 501–507.

49. Keshavarz, M.H.; Jaafari, M. Investigation of the various structure parameters for predicting impact sensitivity of energetic molecules via artificial neural network. *Propellants Explos. Pyrotech.* **2006**, *31*, 216–225. [CrossRef]

50. Nefati, H.; Cense, J.M.; Legendre, J.J. Prediction of the impact sensitivity by neural networks. *J. Chem. Inf. Comput. Sci.* **1996**, *36*, 804–810. [CrossRef]

51. Kuklja, M.M. Quantum-chemical modeling of energetic materials: Chemical reactions triggered by defects, deformations, and electronic excitations. *Adv. Quantum Chem.* **2014**, *69*, 71–146.

52. Sharia, O.; Kuklja, M.M. *Ab Initio* kinetics of gas phase decomposition reactions. *J. Phys. Chem. A* **2010**, *114*, 12656–12661. [CrossRef] [PubMed]

53. Sharia, O.; Kuklja, M.M. Modeling thermal decomposition mechanisms in gaseous and crystalline molecular materials: application to β-HMX. *J. Phys. Chem. B* **2011**, *115*, 12677–12686. [CrossRef] [PubMed]

54. Sharia, O.; Kuklja, M.M. Rapid materials degradation induced by surfaces and voids: *Ab Initio* modeling of β-octatetramethylene tetranitramine. *J. Am. Chem. Soc.* **2012**, *134*, 11815–11820. [CrossRef] [PubMed]

55. Sharia, O.; Kuklja, M.M. Surface-enhanced decomposition kinetics of molecular materials illustrated with cyclotetramethylene-tetranitramine. *J. Phys. Chem. C* **2012**, *116*, 11077–11081. [CrossRef]

56. Hohenberg, P.; Kohn, W. Inhomogeneous electron gas. *Phys. Rev.* **1964**, *136*, B864–B871. [CrossRef]

57. Kohn, W.; Sham, L.J. Self-consistent equations including exchange and correlation effects. *Phys. Rev. A* **1965**, *140*, A1133–A1138.

58. Perdew, J.P.; Burke, K.; Ernzerhof, M. Generalized gradient approximation made simple. *Phys. Rev. Lett.* **1996**, *77*, 3865–3868. [CrossRef] [PubMed]

59. Adamo, C.; Barone, V. Toward reliable density functional methods without adjustable parameters: The PBE0 model. *J. Chem. Phys.* **1999**, *110*, 6158–6169. [CrossRef]

60. Becke, A.D. Density-functional thermochemistry. III. the role of exact exchange. *J. Chem. Phys.* **1993**, *98*, 5648–5652. [CrossRef]

61. Lee, C.; Yang, W.; Parr, R.G. Development of the colle-salvetti correlation-energy formula into a functional of the electron density. *Phys. Rev. B* **1988**, *37*, 785–789. [CrossRef]

62. *Gaussian 09*, Revision B.01 ed; Gaussian, Inc.: Wallingford, CT, USA, 2009.

63. Hratchian, H.P.; Schlegel, H.B. Accurate reaction paths using a hessian based predictor-corrector integrator. *J. Chem. Phys.* **2004**, *120*, 9918–9924. [CrossRef] [PubMed]

64. Hratchian, H.P.; Schlegel, H.B. Using hessian updating to increase the efficiency of a hessian based predictor-corrector reaction path following method. *J. Chem. Theory Comput.* **2005**, *1*, 61–69. [CrossRef] [PubMed]

65. Blöchl, P.E. Projector augmented-wave method. *Phys. Rev. B* **1994**, *50*, 17953–17979. [CrossRef]

66. Kresse, G.; Futhmuller, J. Efficiency of *Ab-initio* total energy calculations for metals and semiconductors using a plane-wave basis set. *Comput. Mater. Sci.* **1996**, *6*, 15–50. [CrossRef]

67. Kresse, G.; Furthmuller, F. Efficient iterative schemes for *Ab initio* total-energy calculations using a plane-wave basis set. *Phys. Rev. B* **1996**, *54*, 11169–11186. [CrossRef]

68. Kresse, G.; Hafner, J. *Ab Initio* molecular dynamics for liquid metals. *Phys. Rev. B* **1993**, *47*, 558–561. [CrossRef]

69. Elban, W.L. Surface energies of high explosives PETN and RDX from contact angle measurements. *J. Mater. Sci.* **1979**, *14*, 1008–1011.

70. Yee, R.Y.; Adicoff, A.; Dibble, E.J. Surface properties of HMX crystal. In Proceedings of the 17th JANNAF Combustion Meeting, Hampton, WV, USA, 22–26 September 1980.

71. Henkelman, G.; Uberuaga, B.P.; Jónsson, H. A climbing image nudged elastic band method for finding saddle points and minimum energy paths. *J. Chem. Phys.* **2000**, *113*, 9901–9904. [CrossRef]

72. Hanggi, P.; Talkner, P.; Borkovec, M. Reaction-rate theory: Fifty years after Kramers. *Rev. Mod. Phys.* **1990**, *62*, 251–341.

73. Garrett, B.C.; Truhlar, D.G. Generalized transition state theory. Classical mechanical theory and applications to collinear reactions of hydrogen molecules. *J. Phys. Chem.* **1979**, *83*, 1052–1079. [CrossRef]

74. Sadhukhan, S.; Muñoz, D.; Adamo, C.; Scuseria, G.E. Predicting proton transfer barriers with density functional methods. *Chem. Phys. Lett.* **1999**, *306*, 83–87. [CrossRef]

75. Nachimuthu, S.; Gao, J.; Truhlar, D.G. A benchmark test suite for proton transfer energies and its use to test electronic structure model chemistries. *Chem. Phys.* **2012**, *400*, 8–12. [CrossRef] [PubMed]

76. See for example, Gruzdkov, Y.A.; Gupta, Y.M. Shock wave initiation of pentaerythritol tetranitrate single crystals: Mechanism of anisotropic sensitivity. *J. Phys. Chem. A* **2000**, *104*, 11169–11176.

77. Zhang, G.; Weeks, B.L.; Zhang, X. Crystal growth of organic energetic materials: Pentaerythritol tetranitrate. *Cent. Eur. J. Eng.* **2012**, *2*, 336–346. [CrossRef]

78. Roos, B.D.; Brill, T.B. Thermal decomposition of energetic materials 82. Correlations of gaseous products with the composition of aliphatic nitrate esters. *Combust. Flame* **2002**, *128*, 181–190. [CrossRef]

79. Ng, W.L.; Field, J.E.; Hauser, H.M. Study of the thermal decomposition of pentaerythritol tetranitrate. *J. Chem. Soc. Perkin Trans.* **1976**, *2*, 637–639. [CrossRef]

80. Andreev, K.K.; Kaidymov, B.I. Thermal decomposition of nitrate esters. II. Thermal decomposition of pentaerythritol tetranitrate. *Russ. J. Phys. Chem.* **1961**, *35*, 1324–1330.

81. Chambers, D.M. *Perspectives on Pentaerythritol Tetranitrate (PETN) Decomposition*; UCRL-JC-148956; Lawrence Livermore National Laboratory: Livermore, CA, USA; July; 2002.

82. Robertson, A.J.B. The thermal decomposition of pentaerythritol tetranitrate, nitroglycerin, ethylenediamine dinitrate and ammonium nitrate. *J. Soc. Chem. Ind.* **1948**, *67*, 221–224. [CrossRef]

83. Rogers, R.N.; Morris, E.D., Jr. On estimating activation energies with a differential scanning calorimeter. *Anal. Chem.* **1966**, *38*, 412–414. [CrossRef]

84. Maycock, J.N.; Pai Verneker, V.R. Characterization of thermal and photosublimation of organic explosives by thermobarogravimetric techniques. *Thermochim. Acta* **1970**, *1*, 191–198. [CrossRef]

85. Volltrauer, H.N. Real time low temperature decomposition of explosives—PETN. *J. Hazard. Mater.* **1982**, *5*, 353–357. [CrossRef]

86. Oxley, J.C.; Smith, J.L.; Brady IV, J.E.; Brown, A.C. Characterization and analysis of tetranitrate esters. *Propellants Explos. Pyrotech.* **2012**, *37*, 24–39. [CrossRef]

87. Tsyshevsky, R.V.; Sharia, O.; Kuklja, M.M. Thermal decomposition mechanisms of nitroesters: *Ab Initio* modeling of pentaerythritol tetranitrate. *J. Phys. Chem. C* **2013**, *117*, 18144–18153. [CrossRef]

88. Liu, W.-G.; Zybin, S.V.; Dasgupta, S.; Klapötke, T.M.; Goddard, W.A., III. Explanation of the colossal detonation sensitivity of silicon pentaerythritol tetranitrate (Si-PETN) explosive. *J. Am. Chem. Soc.* **2009**, *131*, 7490–7491. [CrossRef] [PubMed]

89. Hiskey, M.A.; Brower, K.R.; Oxley, J.C. Thermal decomposition of nitrate esters. *J. Phys. Chem.* **1991**, *95*, 3955–3960. [CrossRef]

90. Choi, C.S.; Boutin, H.P. A study of the crystal structure of β-cyclotetramethylene tetranitramine by neutron diffraction. *Acta. Crystallogr. B* **1970**, *26*, 1235–1240. [CrossRef]

91. Oyumi, Y.; Brill, T.B. Thermal decomposition of energetic materials 3. A high-rate, *in situ*, FTIR study of the thermolysis of RDX and HMX with pressure and heating rate as variables. *Combust. Flame* **1985**, *62*, 213–224. [CrossRef]

92.　Glascoe, E.A.; Hsu, P.C.; Springer, H.K.; de Haven, M.R.; Tan, N.; Turner, H.C. The response of the HMX-based material PBXN-9 to thermal insults: Thermal decomposition kinetics and morphological changes. *Thermochim. Acta.* **2011**, *515*, 58–66. [CrossRef]

93.　Brill, T.B.; James, K.J. Kinetics and mechanisms of thermal decomposition of nitroaromatic explosives. *Chem. Rev.* **1993**, *93*, 2667–2692. [CrossRef]

94.　Brill, T.B.; Gongwer, P.E.; Williams, G.K. Thermal decomposition of energetic materials. 66. Kinetic compensation effects in HMX, RDX, and NTO. *J. Phys. Chem.* **1994**, *98*, 12242–12247. [CrossRef]

95.　Sharia, O.; Tsyshevsky, R.; Kuklja, M.M. Surface-accelerated decomposition of δ-HMX. *J. Phys. Chem. Lett.* **2013**, *4*, 730–734. [CrossRef] [PubMed]

96.　Kuklja, M.M.; Tsyshevsky, R.V.; Sharia, O. Effect of polar surfaces on decomposition of molecular materials. *J. Am. Chem. Soc.* **2014**, *136*, 13289–13302. [CrossRef] [PubMed]

97.　Chakraborty, D.; Muller, R.P.; Dasgupta, S.; Goddard, W.A., III. Mechanism for unimolecular decomposition of HMX (1,3,5,7-tetranitro-1,3,5,7-tetrazocine), an *Ab Initio* study. *J. Phys. Chem. A* **2001**, *105*, 1302–1314. [CrossRef]

98.　Maksimov, Y.Y.; Apol'kova, V.N.; Braverman, O.V.; Solov'ev, A.I. Kinetics of the thermal decomposition of cyclotrimethylenetrinitramine and cyclotetramethylenetetranitramine in the gas phase. *Russ. J. Phys. Chem.* **1985**, *59*, 201–204.

99.　Burov, Y.M.; Nazin, G.M. Influence of structure on rate of decomposition of secondary nitramines in the gas phase. *Kinet. Catal.* **1982**, *23*, 5–10.

100.　Shaw, R.; Walker, F.E. Estimated kinetics and thermochemistry of some initial unimolecular reactions in the thermal decomposition of 1,3,5,7-tetranitro-1,3,5,7-tetraazacyclooctane in the gas phase. *J. Phys. Chem.* **1977**, *81*, 2572–2576. [CrossRef]

101.　Cobbledick, R.E.; Small, R.W.H. The crystal structure of the δ-form of 1,3,5,7-tetranitro-1,3,5,7-tetraazacyclooctane (δ-HMX). *Acta. Crystallogr. B* **1974**, *30*, 1918–1922. [CrossRef]

102.　Herrmann, M.; Engel, W.; Eisenreich, N. Thermal expansion, transitions, sensitivities and burning rates of HMX. *Propellants Explos. Pyrotech.* **1992**, *17*, 190–195. [CrossRef]

103.　Henson, B.F.; Asay, B.W.; Sander, R.K.; Son, S.F.; Robinson, J.M.; Dickson, P.M. Dynamic measurement of the HMX β–δ phase transition by second harmonic generation. *Phys. Rev. Lett.* **1999**, *82*, 1213–1216. [CrossRef]

104.　Henson, B.F.; Smilowitz, L.; Asay, B.W.; Dickson, P.M. The β–δ phase transition in the energetic nitramine octahydro-1,3,5,7-tetranitro-1,3,5,7-tetrazocine: Thermodynamics. *J. Chem. Phys.* **2002**, *117*, 3780–3788. [CrossRef]

105.　Henson, B.F.; Smilowitz, L.; Asay, B.W.; Dickson, P.M. The β–δ phase transition in the energetic nitramine-octahydro-1,3,5,7-tetranitro-1,3,5,7-tetrazocine: Kinetics. *J. Chem. Phys.* **2002**, *117*, 3789–3798. [CrossRef]

106.　Urtiew, P.A.; Forbes, J.W.; Tarver, C.M.; Vandersall, K.S.; Garcia, F.; Greenwood, D.W.; Hsu, P.C.; Maienschein, J.L. Shock sensitivity of LX-04 containing delta phase HMX at elevated temperatures. *AIP Conf. Proc.* **2004**, *706*, 1053–1056.

107.　Asay, B.W.; Henson, B.F.; Smilowitz, L.B.; Dickson, P.M. On the difference in impact sensitivity of β and δ HMX. *J. Energ. Mater.* **2003**, *21*, 223–235. [CrossRef]

108.　Willey, T.M.; Lauderbach, L.; Gagliardi, F.; van Buuren, T.; Glascoe, E.A.; Tringe, J.W.; Lee, J.R.I.; Springer, H.K.; Ilavsky, J. Mesoscale evolution of voids and microstructural changes in HMX-based explosives during heating through the β-δ phase transition. *J. Appl. Phys.* **2015**, *118*. [CrossRef]

109.　Tarver, C.M.; Tran, T.D. Thermal decomposition models for HMX-based plastic bonded explosives. *Combust. Flame* **2004**, *137*, 50–62. [CrossRef]

110.　Brill, T.B.; Karpowicz, R.J. Solid phase transition kinetics. The role of intermolecular forces in the condensed-phase decomposition of octahydro-1,3,5,7-tetranitro-1,3,5,7-tetrazocine. *J. Phys. Chem.* **1982**, *86*, 4260–4265. [CrossRef]

111.　Karpowicz, R.J.; Brill, T.B. Kinetic data for solid phase transitions by Fourier transform infrared spectroscopy. *Appl. Spectrosc.* **1983**, *37*, 79–81. [CrossRef]

112.　Whelan, D.J.; Fitzgerald, M.R. *A Reassessment of the Kinetics of the Thermal Decomposition of the High Explosive, Delta-HMX, in the Range 508 K to 524 K, as Studied by Isothermal Gravimetry*; DSTO-TR-0635; DSTO Aeronautical and Maritime Research Laboratory: Melbourne, Australia, 1998.

113. Bulusu, S.; Weinstein, D.I.; Autera, J.R.; Velicky, R.W. Deuterium kinetic isotope effect in the thermal decomposition of 1,3,5-trinitro-1,3,5-triazacyclohexane and 1,3,5,7-tetranitro-1,3,5,7-tetraazacyclooctane: its use as an experimental probe for their shock-induced chemistry. *J. Phys. Chem.* **1986**, *90*, 4121–4126. [CrossRef]

114. Fox, P.G.; Hutchinson, R.W. Slow thermal decomposition. In *Energetic Materials, Physics and Chemistry of Inorganic Azides*; Fair, H.D., Walker, R.F., Eds.; Plenum Press: New York, NY, USA, 1977; p. 255.

115. Latypov, N.V.; Bergman, J.; Langlet, A.; Wellmar, U.; Bemm, U. Synthesis and reactions of 1,1-diamino-2,2-dinitroethylene. *Tetrahedron* **1998**, *54*, 11525–11536. [CrossRef]

116. Bemm, U.; Östmark, H. 1,1-Diamino-2,2-dinitroethylene: A novel energetic material with infinite layers in two dimensions. *Acta. Crystallogr.* **1998**, *C54*, 1997–1999. [CrossRef]

117. Östmark, H.; Langlet, A.; Bergman, H.; Wingborg, U.; Wellmar, U.; Bemm, U. FOX-7—A new explosive with low sensitivity and high performance. In Proceedings of 11th International Symposium on Detonation, Snowmass, CO, USA, 1998.

118. Lochert, I.J. *FOX-7—A New Insensitive Explosive*; ADA399359; DSTO Aeronautical and Maritime Research Laboratory: Fishermans Bend, Australia; November; 2001.

119. Burnham, A.K.; Weese, R.K.; Wang, R.; Kwok, Q.S.M.; Jones, D.E.G. Thermal properties of FOX-7. In Proceedings of the 36th International Annual Conference of ICT & 32nd International Pyrotechnics Seminar, Karlsruhe, Germany, 28 June–1 July 2005.

120. De Klerk, W.; Popescu, C.; van der Heijden, A. Study on the decomposition kinetics of FOX-7 and HNF. *J. Therm. Anal. Cal.* **2003**, *72*, 955–966. [CrossRef]

121. Politzer, P.; Concha, M.C.; Grice, M.E.; Murray, J.S.; Lane, P.; Habibollazadeh, D. Computational investigation of the structures and relative stabilities of amino/nitro derivatives of ethylene. *Theochem. J. Mol. Struct.* **1998**, *452*, 75–83. [CrossRef]

122. Kimmel, A.V.; Sushko, P.V.; Shluger, A.L.; Kuklja, M.M. Effect of charged and excited states on the decomposition of 1,1-diamino-2,2-dinitroethylene molecules. *J. Chem. Phys.* **2007**, *126*, 234711–234721. [CrossRef] [PubMed]

123. Gindulyte, A.; Massa, L.; Huang, L.; Karle, J. Proposed mechanism of 1,1-diamino-dinitroethylene decomposition: a density functional theory study. *J. Phys. Chem. A* **1999**, *103*, 11045–11051. [CrossRef]

124. Kuklja, M.M.; Rashkeev, S.N. Self-accelerated mechanochemistry in nitroarenes. *J. Phys. Chem. Lett.* **2010**, *1*, 363–367. [CrossRef]

125. Booth, R.S.; Butler, L.J. Thermal decomposition pathways for 1,1-diamino-2,2-dinitroethene (FOX-7). *J. Chem. Phys.* **2014**, *141*. [CrossRef] [PubMed]

126. Kiselev, V.G.; Gritsan, N.P. Unexpected primary reactions for thermolysis of 1,1-diamino-2,2-dinitroethylene (FOX-7) revealed by *Ab Initio* calculations. *J. Phys. Chem. A* **2014**, *118*, 8002–8008. [CrossRef] [PubMed]

127. Gibbs, T.R., Popolato, A., Eds.; *LASL Explosive Property Data*; University of California Press: Oakland, CA, USA, 1980.

128. Rogers, R.N.; Janney, J.L.; Ebinger, M.H. Kinetic-isotope effects in thermal explosions. *Thermochim. Acta* **1982**, *59*, 287–297. [CrossRef]

129. Stolovy, A.; Jones, E.C., Jr.; Aviles, J.B., Jr.; Namenson, A.I.; Fraser, W.A. Exothermic reactions in TATB initiated by an electron beam. *J. Chem. Phys.* **1983**, *78*, 229–235. [CrossRef]

130. Wu, C.J.; Fried, L.E. Ring closure mediated by intramolecular hydrogen transfer in the decomposition of a push-pull nitroaromatic: TATB. *J. Phys. Chem. A* **2000**, *104*, 6447–6452. [CrossRef]

131. Shao, J.; Cheng, X.; Yang, X. The C−NO$_2$ bond dissociation energies of some nitroaromatic compounds: DFT study. *Struct. Chem.* **2006**, *17*, 547–550. [CrossRef]

132. Manaa, M.R.; Fried, L.E. The reactivity of energetic materials under high pressure and temperature. In *Energetic Materials*; Sabin, J.R., Ed.; Academic Press: Cambridge, MA, USA, 2014.

133. Kimmel, A.V.; Sushko, P.V.; Shluger, A.L.; Kuklja, M.M. Effect of molecular and lattice structure on hydrogen transfer in molecular crystals of diamino-dinitroethylene and triamino-trinitrobenzene. *J. Phys. Chem. A* **2008**, *112*, 4496–4500. [CrossRef] [PubMed]

134. Tsyshevsky, R.; Pagoria, P.; Zhang, M.; Racoveanu, A.; de Hope, A.; Parrish, D.; Kuklja, M.M. Searching for low-sensitivity cast-melt high-energy-density materials: Synthesis, characterization, and decomposition kinetics of 3,4-bis(4-nitro-1,2,5-oxadiazol-3-yl)-1,2,5-oxadiazole-2-oxide. *J. Phys. Chem. C* **2015**, *119*, 3509–3521. [CrossRef]

135. Zhao, F.Q.; Chen, P.; Hu, R.Z.; Luo, Y.; Zhang, Z.Z.; Zhou, Y.S.; Yang, X.W.; Gao, Y.; Gao, S.L.; Shi, Q.Z. Thermochemical properties and non-isothermal decomposition reaction kinetics of 3,4-dinitrofurazanfuroxan (DNTF). *J. Hazard. Mater.* **2004**, *113*, 67–71.

136. Zeldovich, Y.B. *On The Theory of the Propagation of Detonations on Gaseous System*; NACA-TM-1261; National Advisory Committee for Aeronautics: Washington, DC, USA, 1950. (In Russian)

137. Von Neumann, J. *Theory of Detonation Waves*; ADB967734; Institute for Advanced Study: Princeton, NJ, USA, 1942.

138. Lee, E.L.; Tarver, C.M. Phenomenological model of shock initiation in heterogeneous explosives. *Phys. Fluids* **1980**, *23*. [CrossRef]

139. McGuire, R.R.; Tarver, C.M. Chemical-Decomposition Models for the Thermal Explosion of Confined HMX, TATB, RDX, and TNT Explosives. In Proceedings of the 7th Symposium (International) on Detonation, Annapolis, MD, USA, 16–19 June 1981.

140. Tarver, C.M.; Forbes, J.W.; Urtiew, P.A. Nonequilibrium Zeldovich-von Neumann-Doring theory and reactive flow modeling of detonation. *Russ. J. Phys. Chem. B* **2007**, *1*, 39–45. [CrossRef]

141. Kuklja, M.M.; Rashkeev, S.N. Interplay of decomposition mechanisms at shear-strain interface. *J. Phys. Chem. C* **2009**, *113*, 17–20. [CrossRef]

142. Tsyshevsky, R.V.; Rashkeev, S.N.; Kuklja, M.M. Defect states at organic-inorganic interfaces: Insight from first principles calculations for pentaerythritol tetranitrate on MgO surface. *Surf. Sci.* **2015**, *19*, 637–638. [CrossRef]

143. Tsyshevsky, R.V.; Zverev, A.; Mitrofanov, A.; Rashkeev, S.N.; Kuklja, M.M. Photochemistry of the α-Al$_2$O$_3$-PETN interface. *Molecules* **2016**, submitted for publication.

144. Aluker, E.D.; Krechetov, A.G.; Mitrofanov, A.Y.; Nurmukhametov, D.R.; Kuklja, M.M. Laser initiation of energetic materials: Selective photoinitiation regime in pentaerythritol tetranitrate. *J. Phys. Chem. C* **2011**, *115*, 6893–6901. [CrossRef]

145. Aluker, E.D.; Krechetov, A.G.; Mitrofanov, A.Y.; Zverev, A.S.; Kuklja, M.M. Understanding limits of the thermal mechanism of laser initiation of energetic materials. *J. Phys. Chem. C* **2012**, *116*, 24482–24486. [CrossRef]

146. Aluker, E.D.; Krechetov, A.G.; Mitrofanov, A.Y.; Zverev, A.S.; Kuklja, M.M. Topography of photochemical initiation in molecular materials. *Molecules* **2013**, *18*, 14148–14160. [CrossRef] [PubMed]

147. Wang, Y.A.; Carter, E.A. Orbital-free kinetic-energy density functional theory. In *Theoretical Methods in Condensed Phase Chemistry*; Schwartz, S.D., Ed.; Springer: Dordrecht, The Netherlands, 2002; pp. 117–184.

148. Vikram, G.; Bhattacharya, K.; Ortiz, M. Quasi-continuum orbital-free density-functional theory: A route to multi-million atom non-periodic DFT calculation. *J. Mech. Phys. Solids* **2007**, *55*, 697–718.

149. Dreizler, R.M.; Gross, E.K.U. *Density Functional Theory: An Approach to the Quantum Many-Body Problem*; Springer-Verlag: Berlin, Germany, 2012; p. 304.

150. Taylor, D.E.; Rice, B.M. Quantum-informed multiscale M & S for energetic materials. In *Energetic Materials*; Sabin, J.R., Ed.; Academic Press: Cambridge, MA, USA, 2014.